SAND2018-6731J

Automatic signal decoding and sensor stability of a 3-electrode mixed-potential sensor for NO_x/NH_3 quantification

Lok-kun Tsui[a,*], Angelica Benavidez[a], Ponnusamy Palanisamy[b], Lindsey Evans[c], Fernando Garzon[a,c]

[a] Center for MicroEngineered Materials, University of New Mexico, Albuquerque, New Mexico, 87106, USA
[b] ESL ElectroScience, King of Prussia, Pennsylvania, 19406, USA
[c] Advanced Materials Laboratory, Sandia National Laboratories, Albuquerque, New Mexico, 87106, USA

Abstract

Sensors to detect mixtures of NO_x/NH_3 are needed to monitor emissions of diesel automobiles where a selective catalytic reduction system uses an NH_3 mediated reaction to reduce NO_x. We report on the application of a three electrode $La_{0.8}Sr_{0.2}CrO_3$, $Au_{0.5}Pd_{0.5}$, Pt mixed potential sensor using yttria-stabilized-zirconia (YSZ) as a solid electrolyte to NO_x/NH_3 sensing. Artificial neural networks were used to automatically decode the concentrations of NO_x/NH_3 and errors of less than 15% are achieved. The optimal architecture for ANN decoding and the maximum density of training data points are also determined. The stability of the sensor was monitored by electrochemical impedance spectroscopy. The impedance associated with YSZ oxygen ion conduction and the electrochemical reactions at the three-phase interface are tracked over a period of over 100 days.

Keywords: NO_x; NH_3; mixed potential sensor; artificial neural network

Corresponding Author: Lok-kun Tsui (lktsui@unm.edu)
Mailing Address: 1001 University Blvd SE, Center for MicroEngineered Materials, Albuqerque, NM, 87106

1. Introduction

Lean burn diesel engines can achieve higher fuel efficiency but require a complex catalytic reaction system to control hydrocarbon (HC), CO, and NO_x emissions.[1] NO_x has been identified as an environmental pollutant causing ozone damage and acid rain as well as a harmful chemical to the respiratory system.[2] Selective catalytic reduction (SCR) uses urea (NH_2-CO-NH_2) which is converted into NH_3 (equation 1) to mediate a reduction reaction of NO_x (NO or NO_2) to N_2 by the reactions in equations 2 and 3 [3,4]. At the end of the emissions treatment stream excess NH_3 is eliminated at the ammonia oxidation catalyst (AOC) reactor producing N_2 in equation 4.

$$NH_2\text{-}CO\text{-}NH_2 + H_2O \rightarrow 2NH_3 + CO_2 \quad [1]$$

$$4\ NH_3 + 4\ NO + O_2 \rightarrow 4\ N_2 + 6\ H_2O \quad [2]$$

$$4\ NH_3 + 2\ NO_2 + O_2 \rightarrow 3\ N_2 + 6\ H_2O \quad [3]$$

$$4\ NH_3 + 3\ O_2 \rightarrow 2\ N_2 + 6\ H_2O \quad [4]$$

There is a need to develop sensors to quantitatively and continuously monitor their performance in real time.[5] Deploying sensors which can monitor the emissions of NO_x and NH_3 at the output of the exhaust stream would enable the fine tuning of these catalytic systems in real time for improved efficiency and alert the vehicle owner of problems without requiring an external emissions measurement.

The numerous approaches to the design of NH_3 / NO_x sensors in the literature have involved semiconductor metal oxide sensors and mixed potential sensors using conductivity, amperometry, or voltammetry as sensing parameters. [6–9] Currently there is no commercially available automotive sensor which is capable of measuring the NH_3/NO_x concentration simultaneously in exhaust gases. Cross interference between the signals in the presence of both NO_x and NH_3 have driven a substantial amount of research towards sensors

which are strongly selective towards either NO_x or NH_3. These methods include measuring the conductivity of zeolites engineered to be sensitive towards the target gas [10] and coating a sensor with a catalytic layer to filter out unwanted gas species [11]. Arrays of metal oxide sensor elements have also been studied where each element is to be sensitive to a specific gas by changing the noble metal doping and substrate.[12]

Mixed potential electrochemical sensors are one of the most promising technologies for use in automotive emissions control because of their high stability in the environment, fast response, and tunable selectivity to a broad range of target gases by materials selection or current biasing. The mixed potential on each electrode is determined by the balance between the reduction and oxidation reactions of the gases present in the atmosphere. A difference in mixed potentials due to the different catalytic activities of the electrode materials can then be used as a sensing parameter on oxidizable (HC, CO, NH_3) or reducible gases (NO_x).[13,14] Au/YSZ/Pt sensors have been identified as effective for detection of NH_3, while $La_{0.8}Sr_{0.2}CrO_3$ (LSCO)/YSZ/Pt sensors are sensitive to hydrocarbons under open circuit and sensitive to NO_x under an applied bias.[15,16] We have designed a three-electrode mixed potential sensor incorporating LSCO, $Au_{0.5}Pd_{0.5}$ (Au/Pd) alloy, and Pt electrodes with an over layer of porous YSZ electrolyte. The sensor has an integrated Pt thin film heater on the back, which controls the temperature by an applied bias.

Quantitative decoding of the sensor responses of mixed potential electrochemical sensors to NO_x/NH_3 in the presence of cross interference remains an unsolved challenge. Tsitron et al. and Ramaiyan et al. have pursued a Bayesian approach to quantify the ratio of concentrations in a binary mixtures of NO_x, C_3H_8, and NH_3.[17,18] This approach started with linear and logarithmic functional relationships between concentration and voltage and Bayesian inference was used to obtain the fitting parameters. We have previously explored an alternative approach involving artificial neural networks (ANNs) to quantify binary and ternary concentrations of NO, C_3H_8, and CO,[19,20] and in this report we extend this work to quantification of NH_3 and NO_x. A major advantage of ANNs is that they do not require specification of functional forms in advance as these structures can take advantage of their ability to automatically learn the relationships between sensor responses and species concentrations from a training dataset. This feature

allows the network to easily scale the automatic analysis with an increasing number of signal inputs and cross-interference effects that are introduced with the addition of more gases into the mixture. The application of this technique to a new set of gas mixtures also demonstrates its versatility and shows that the same sensor can be used to analyze gas species at different stages of the exhaust treatment pipeline.

We report the extraction of concentrations of NH_3 and NO_x ($NO+NO_2$) from sensor signals automatically using an artificial neural network. By operating the sensor in unbiased mode, we are able to increase sensitivity to NH_3, while operating in biased mode provides sensitivity to NO_x. As a result, we are able to achieve a total peak error of 5% in the concentration of NO_x and NH_3 with 90% of test data points confined to less than 15% error. The stability of the sensor is also monitored for over 3 months and impedance spectroscopy was used to track changes in the resistance of the YSZ and resistance associated with the electrochemical reactions at the three-phase interface.

2. Materials and Methods

Sensors were constructed by ESL ElectroScience on laminated tapes of YSZ substrates coated with an insulating ceramic layer. A serpentine thin film Pt heater element on the rear and dense electrodes made of Pt, $Au_{0.5}Pd_{0.5}$, LSCO with a porous YSZ electrolyte on the front were deposited by screen printing. The electrodes are evenly spaced and the Au/Pd electrode is located between the Pt and LSCO electrodes. The sintering temperatures for Pt electrodes and heater path, LSCO electrodes, Au/Pd electrode, and YSZ electrolytes are 1450°C, 1200°C, 1100°C, and 1100°C respectively.

Contacts to the elements were made by Ag-Sn soldering Ag wires to the electrode elements and Cu wires to the rear heater unit. The wires were threaded through alumina tubes and JB Weld epoxy was used to reinforce the connections against mechanical stress. Two sensors were inserted into 1" glass tubes. The sensors are heated from two of the outputs of an HP 6627A quad-output power supply to 530°C by applying a voltage of 14V. Gas mixing is controlled by an Environics 2000 gas mixing system, and a schematic of the gas mixing and test system is available in ref. [20]. Voltages across each of the electrode pairs are

recorded by two Keithley 2400 digital sourcemeters, a Fluke 8842A digital multimeter, and three HP 34401A digital multimeters with the following polarity convention: Au/Pd(+) and Pt(-), LSCO(+) and Pt(-), Au/Pd(+) and LSCO(-). One sensor is left at open circuit while the second sensor is held at an applied current bias of -0.6 μA to the LSCO/Pt pair.

The sensors were exposed to a gas mixture consisting of a base gas of 10% O_2, 2.5% CO_2, and balance nitrogen. Binary mixtures of NH_3 with NO or NO_2 were obtained in concentration windows of 50-200 ppm. Ternary mixtures of NH_3 with NO_x (NO and NO_2) were obtained in concentration windows of 50-150ppm. The flow rate from the gas mixer was set to 220 SCCM and split to 110 SCCM per sensor. The sensors were exposed to alternating 10 minute intervals of base gas only and base gas with test gas.

We trained artificial neural networks to take the voltage readings from the biased and unbiased sensor as inputs and output the NO_x/NH_3 concentrations. A Python 2.7.3 neural network library Keras with the Theano back-end in CPU mode was used for building artificial neural networks.[21] Fully connected, feed-forward artificial neural networks were constructed using the architecture in Figure 1 with 6 input neurons, 16 hidden layer neurons, and two output neurons. The activation function used was sigmoidal with bias. Prior to analysis, voltage readings were normalized to 100 mV and concentrations were normalized to 200 ppm. The voltage input was then stretched so that the variance of the training data was unity. The voltages were provided to the input side of the neural network, and the normalized concentrations were obtained from the output of the neural network. A total of 159 data points was collected for binary mixtures of NH_3 and NO or NO_2 and 215 data points were collected from ternary mixtures of NH_3 and varying ratios of $NO:NO_2$ in NO_x. A total of 10^4 iterations of training were performed with the Keras's built-in ADAM training algorithm with a runtime of 20-70 seconds on a desktop PC with an Intel i5-6500 processor. To assess how well the artificial neural network generalizes, the datasets were processed with 10 iterations of randomly partitioning into test-training splits at a ratio of 80% training data and 20% test data.

Contour plots of the behavior of the neural networks were generated by principle component analysis (PCA) following the process outlined in ref. [20] using the method of covariance matrices and singular value

decomposition. The 6D sensor signal data points are projected down into a 2D plane in order to be represented in an image. The contour plots are generated by sampling the 2D plane, determining the equivalent 6D sensor reading, and obtaining a prediction of concentration from the neural network. This allows us to visualize whether the predicted concentrations qualitatively match with trends as one moves around in 2D PCA space.

Additional electrochemical measurements were collected using a PAR 2273 potentiostat to assess the robustness of the sensor overtime and examine the behavior of the 3-electrode sensor under applied current bias. Electrochemical impedance spectroscopy was collected at open circuit between 2 MHz and 0.1 Hz with an applied sinusoidal perturbation of 10 mV. The robustness of the sensors was evaluated by exposing the sensor to 50-200 ppm of NO, NO_2, NH_3, and 75-250 ppm of C_3H_8 alternating between running the sensor in unbiased and under current bias mode. Between each measurement, impedance measurements were made for all three pairs of electrodes and fit to the equivalent circuit model shown in Figure 2.

3. Results and Discussion

3.1 Sensor Response to NO_x and NH_3

Figure 3 shows the voltage responses of all three electrode pairs with the sensor in open circuit and LSCO/Pt biased mode to concentrations of NH_3 between 50 and 225 ppm at 0, 100, and 200 ppm of NO or NO_2. Figure S1 in the Supplementary Information provides the plots with NH_3 concentration on a linear scale. Baseline voltages for all three electrode pairs on the sensors operating in open circuit mode were < 5 mV. Under applied bias, the baseline voltage was -215 mV for LSCO/Pt, -60 mV for AuPd/Pt, and +114 mV for AuPd/LSCO. The strongest response to NH_3 is from the Au/Pd+Pt electrode pair on the unbiased sensor which exhibits a response change of 60 mV between the minimum and maximum concentrations. The response of NH_3 is suppressed on the LSCO+Pt pair on the biased sensor while the signal from the NO_x species is enhanced. At the lower limit of NH_3 concentration, the signal response to NO_2 is 60 mV while that for NO is 35 mV. In both NO and NO_2 sensitivity to under applied bias is weaker when the

concentration of NH_3 is at its maximum. A voltage difference of only 25 mV is seen in NO_2 and 15 mV for NO. Deviations from linearity are observed in the high concentrations of NO_2 in the presence of NH_3 on the LSCO+Pt and Au/Pd+Pt sensor pairs and indicates a cross interference effect on these sensing electrodes. The neural networks explored later in this manuscript will be tasked with automatically deconvoluting them. The time response for NO_x and NH_3 is shown in Supplementary Information Figure S2. The time needed to reach a steady state voltage upon exposure to a new test gas and the return to baseline is approximately 10 minutes for all six electrode pairs. We have chosen an operating temperature of 530°C as a compromise between response speed and signal intensity since signal intensity is diminished with increasing temperature. The mixed potential sensors of this type have previously been demonstrated by Kreller et al. to respond quickly enough to track the concentration of NO_x in real time under dynamometer testing at flow rates on the order of 5-35 liters per minute than can be achieved with our mass flow controllers[22]. The delay observed in our sensor response can be partially attributed to the relatively weak flow rate (110 SCCM per sensor) compared to the result from Kreller et al.

3.2 ANN Decoding of Sensor Response

We first examined binary mixtures of NO_2 or NO with NH_3 to determine whether a single neural network could be generalized to both NO_2 and NO. If this is possible, a pre-separation step of data into $NO+NH_3$, NO_2+NH_3, or $NO_2+NO+NH_3$ will not be necessary. Figure 4 shows the results of artificial neural network analysis of binary mixture concentrations of NO_2 and NO with NH_3. Networks trained on separated binary mixtures produce peak error of 5%. When one neural network is tasked with taking a combined dataset of NO_2+NH_3 and $NO+NH_3$ to produce concentrations of total NO_x and NH_3, the resulting peak error distribution is broader but the maximum remains at 5%. These results demonstrate that it is not necessary to construct separate ANNs for mixtures rich in NO, mixtures rich in NO_2, and mixtures with ternary mixtures of $NO+NO_2+NH_3$.

The optimum ANN model is a function of the size of the ANN hidden layer. Increasing the hidden layer size provides a better fit to the experimental data, but increasing the complexity also increases processing

time and the ANN may overfit the training data and poorly generalize to previously unseen signals. Figure 5(a) shows the test and training errors as a function of the size of the hidden layer (HL) for ternary mixtures of NO, NO_2, and NH_3. Diminishing returns are reached after 16 HL neurons are used. For the remainder of the data presented in this paper, all neural networks are constructed in a 16 neuron HL configuration. Increasing the size of the training dataset will also improve the calibration of the neural networks. Figure 5(b) shows that the concentration test error does not improve after 150 data points are collected, which implies that collecting a density of points higher than 12 pts per 50 ppm NO_x x 50 ppm NH_3 window is redundant.

The results for the ternary mixtures are shown in Figure 6 with concentration errors broken down into NO_x error, NH_3 error, and a combined error metric. The concentration error for 90% of test data points is 20% for NO_x, 7% for NH_3, and 15% total concentration error. These results indicate much greater accuracy for NH_3 compared to NO_x. The data that is obtained from the 6 sensor electrode pairs corresponds to a 6D dataset, and we use principle component analysis (PCA) to project this down into a 2D plane for visualization. The distribution of voltage signals as a function of concentration is visualized in Figure 7 by PCA plots with darker markers indicating higher concentrations. The contours projected over the PCA data are a result of taking points in 2D PCA space and projecting them up to 6D space to feed to the artificial neural network to generate concentration predictions. The data from NO_x in Figure 7(a) shows that moving towards the top left is associated with increased NO_x concentrations but there is more scatter and noise in this dataset than there is in the NH_3 data. This may also indicate that accurate predictions on NO_x require higher dimensional data which cannot be represented on a 2D plane. In contrast, the NH_3 dataset in Figure 7(b) shows a clear trend towards increased concentration moving as voltage signals move towards the top right. The contours show that the artificial neural networks are able to produce maps from voltage to concentration in 2D PCA space which appear reasonable to human inspection.

3.3 Sensor Stability

Representative impedance spectra for each of the three electrode pairs taken during the middle of the endurance experiment are shown in Figure 8(a). Two time constants are observed: a semicircular arc that appears at high frequencies (R1/C1) and a depressed arc that occurs at higher frequencies (R2/Q2). The conduction of the oxygen ions through the YSZ electrolyte is assigned to the high frequency arc, while the gas reactions impedance is associated with the lower frequency arc. Figure 8(b) and 8(c) show the R1 and R2 impedance as a function of time. The sensor underwent several stages where it had to be unloaded from the test system and brought to room temperature as indicated by the white areas of Figures 8(b) and 8(c), but neither resistance is affected by this process. The R1 resistance is stable throughout the entire test period at 120 kΩ for LSCO/Pt and 60 kΩ for Au/Pd+Pt and AuPd+LSCO respectively. High stability is also observed in the impedance for Au/Pd+Pt's R2 resistance, remaining fixed at 50 kΩ throughout the course of the endurance test. The LSCO electrode pairs exhibit an initial decay over an initial 30 days, followed by a period of stability at 300 kΩ during the remainder of the experiment. The initial decay may be a result slow sintering of the electrodes under operational temperature which would alter the exposed surface area and catalytic properties of the electrodes. This indicates an initial break-in period or more optimized initial sintering during fabrication may be necessary to establish stability in the LSCO electrode.

4. Conclusions

We have demonstrated that our three-electrode mixed potential sensor can be used to quantify mixtures of NO_x and C_3H_8 assisted by artificial neural networks to perform signal analysis. The optimal number of hidden layer neurons and the maximum density of data points was determined. The distribution of errors produced by the ANN method had a peak at 5% error and 90% of test data points confined to15% total error. Finally, the stability of the sensor was investigated for a period of over 100 days using electrochemical impedance spectroscopy. The YSZ electrolyte and Au-Pd electrode showed high stability throughout the test, while the LSCO electrode needs an initial break-in period to achieve acceptable stability.

Acknowledgments

We acknowledge funding from the University of New Mexico Center for MicroEngineered Materials and the Sandia National Laboratories LDRD program through funding code DE-AC04-94-AL85000.

Conflict of Interest Statement

Declaration of Interest: None

5. References

[1] M. V. Twigg, Appl. Catal. B Environ. 70 (2007) 2–15.

[2] S. Roy, M.S. Hegde, G. Madras, Appl. Energy 86 (2009) 2283–2297.

[3] G. Busca, L. Lietti, G. Ramis, F. Berti, Appl. Catal. B Environ. 18 (1998) 1–36.

[4] M. Koebel, M. Elsener, M. Kleemann, Catal. Today 59 (2000) 335–345.

[5] A. Walker, Top. Catal. 59 (2016) 695–707.

[6] X. Wang, N. Miura, N. Yamazoe, Sensors Actuators, B Chem. 66 (2000) 74–76.

[7] C.N. Xu, N. Miura, Y. Ishida, K. Matsuda, N. Yamazoe, Sensors Actuators, B Chem. 65 (2000) 163–165.

[8] Y. Takao, J. Electrochem. Soc. 141 (1994) 1028.

[9] C. Imawan, F. Solzbacher, H. Steffes, E. Obermeier, Sensors Actuators B Chem. 64 (2000) 193–197.

[10] R. Moos, R. Müller, C. Plog, A. Knezevic, H. Leye, E. Irion, T. Braun, K.J. Marquardt, K. Binder, Sensors Actuators, B Chem. 83 (2002) 181–189.

[11] D. Schönauer, K. Wiesner, M. Fleischer, R. Moos, Sensors Actuators, B Chem. 140 (2009) 585–590.

[12] B.T. Marquis, J.F. Vetelino, Sensors Actuators, B Chem. 77 (2001) 100–110.

[13] F.H. Garzon, R. Mukundan, E.L. Brosha, Solid State Ionics 136–137 (2000) 633–638.

[14] J.W. Fergus, J. Solid State Electrochem. 15 (2011) 971–984.

[15] P.K. Sekhar, E.L. Brosha, R. Mukundan, W. Li, M.A. Nelson, P. Palanisamy, F.H. Garzon, Sensors Actuators, B Chem. 144 (2010) 112–119.

[16] R. Mukundan, K. Teranishi, E.L. Brosha, F.H. Garzon, Electrochem. Solid-State Lett. 10 (2007) J26.

[17] J. Tsitron, C.R. Kreller, P.K. Sekhar, R. Mukundan, F.H. Garzon, E.L. Brosha, A. V. Morozov, Sensors Actuators B Chem. 192 (2013) 283–293.

[18] K. Ramaiyan, C.R. Kreller, E.L. Brosha, R. Mukundan, U. Javed, A. V Morozov, ECS Trans. 75 (2016) 107–111.

[19] L. -k. Tsui, A.D. Benavidez, P. Palanisamy, L. Evans, F.H. Garzon, ECS Trans. 75 (2016) 9–22.

[20] L. Tsui, A. Benavidez, P. Palanisamy, L. Evans, F. Garzon, Sensors Actuators B Chem. 249 (2017) 673–684.

[21] F. Chollet, Github (2015).

[22] C.R. Kreller, P.K. Sekhar, V. Prikhodko, J. Pihl, S. Curran, J.E. Parks, R. Mukundan, F. Garzon, E.L. Brosha, ECS Trans. 61 (2014) 55–63.

Figures

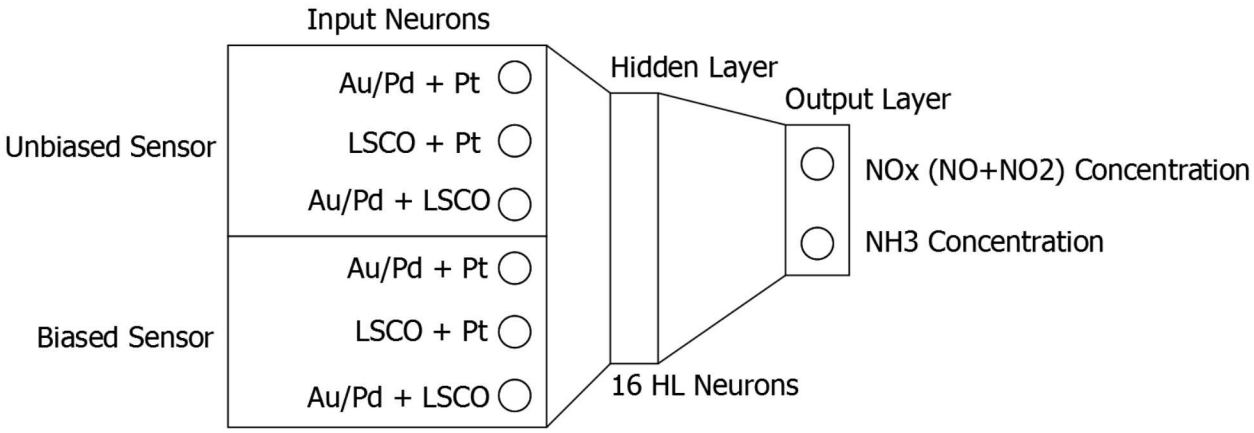

Figure 1. Fully connected, feed forward artificial neural network structure which takes voltage readings from the biased and unbiased sensor and outputs the NO_x/NH_3 concentrations.

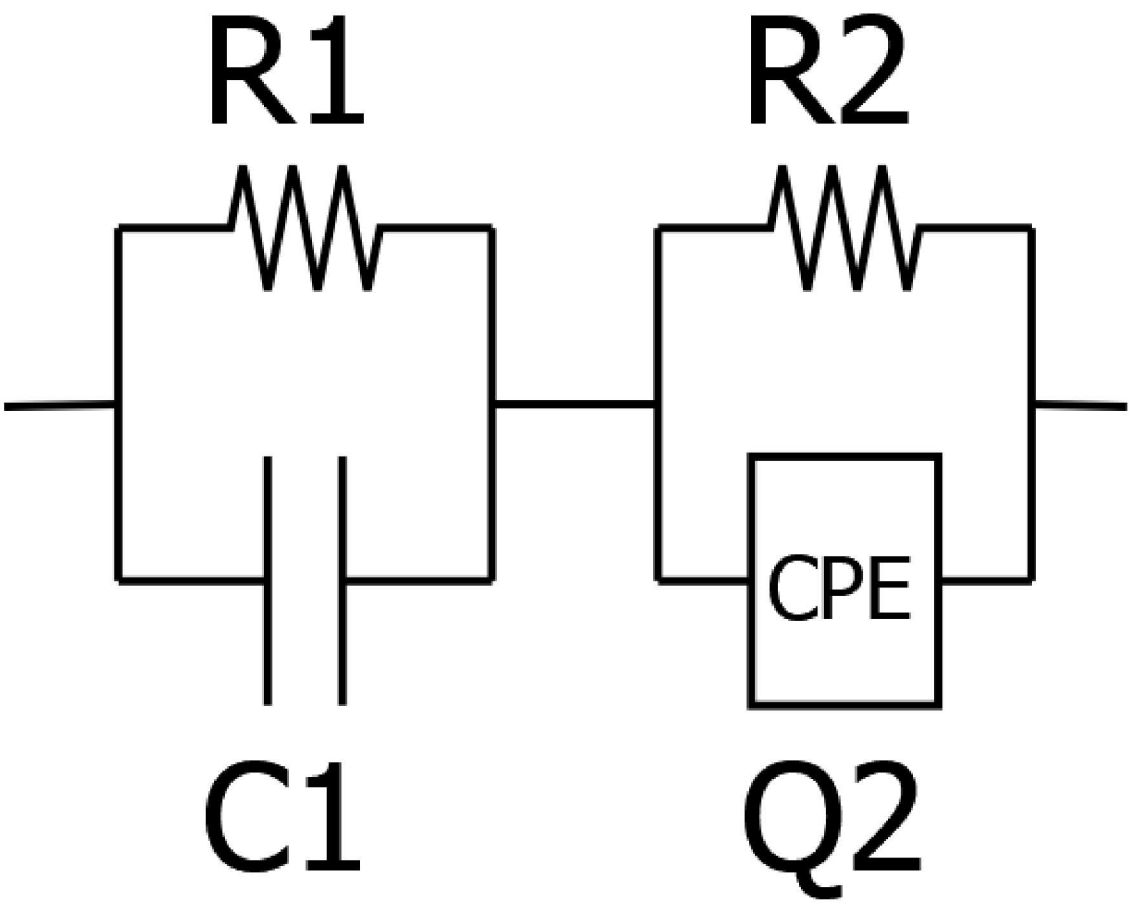

Figure 2. Equivalent circuit model for EIS measurements made on the three-electrode sensor. R represents a resistor, C represents a capacitor, and Q represents a constant phase element (CPE).

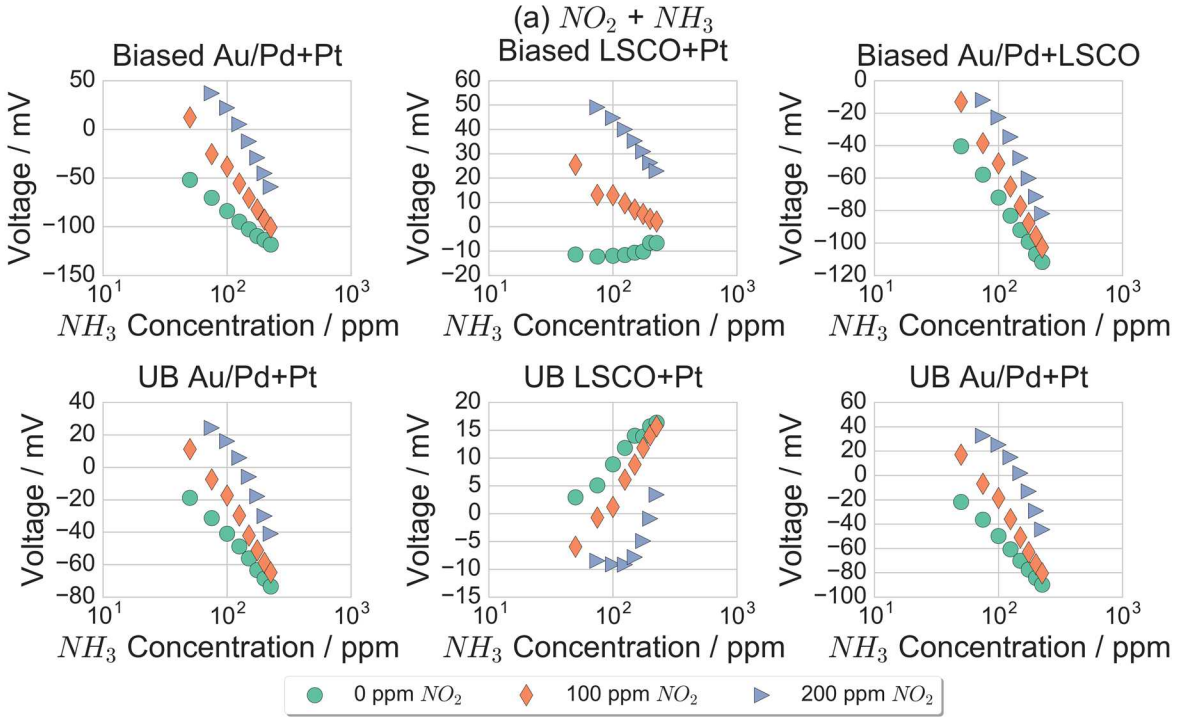

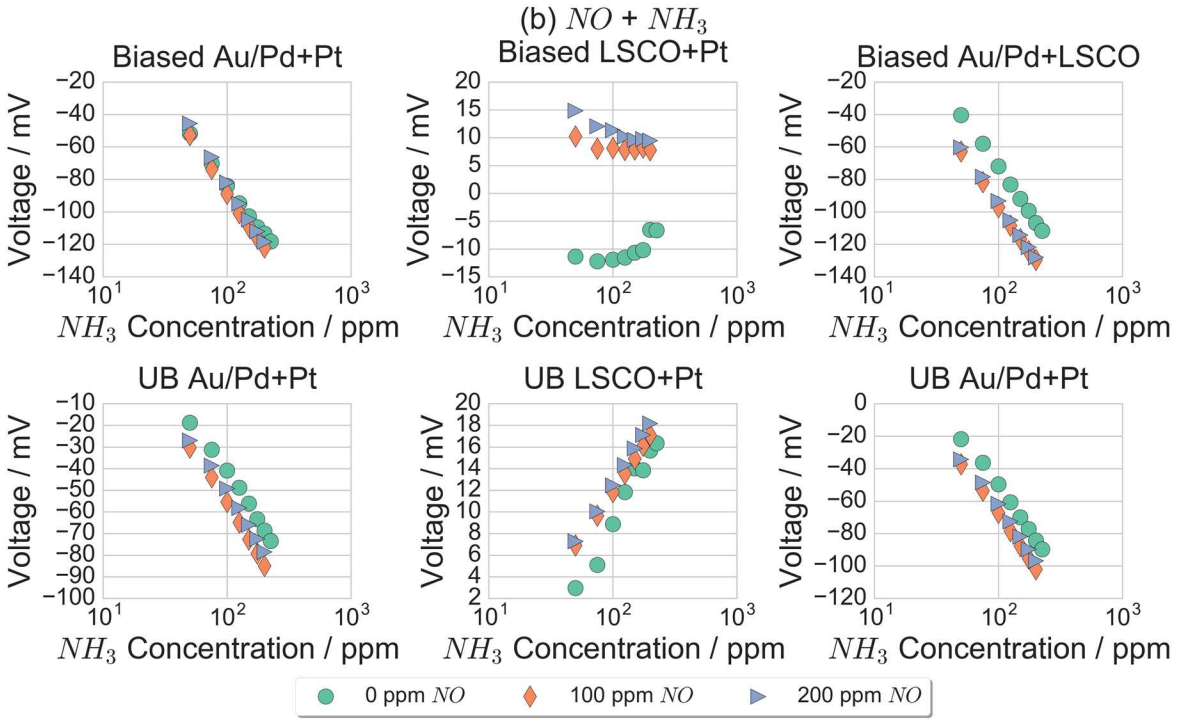

Figure 3. Voltage response to binary mixtures of (a) NO_2 and NH_3 and (b) NO and NH_3. The signals are collected on the unbiased (UB) sensor and the sensor with a current bias applied to the LSCO/Pt pair

(Biased). The signal for NH_3 is suppressed under applied bias while the signal for the NO_x species are enhanced.

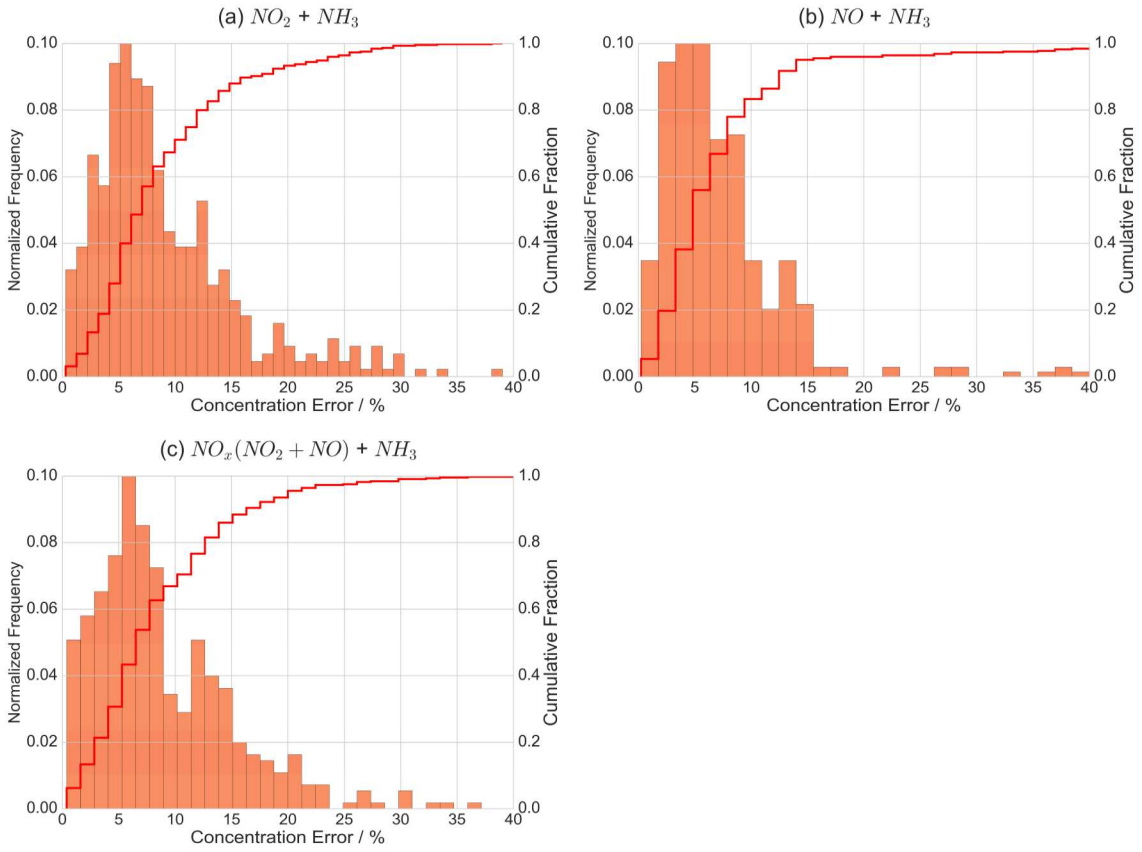

Figure 4. Error histograms for test datasets generated by repeated subsampling cross validation for binary mixtures of (a) NO_2 + NH_3, (b) NO + NH_3. (c) Shows the error histogram generated by combining the two binary mixture datasets and generating predictions of total NO_x and NH_3.

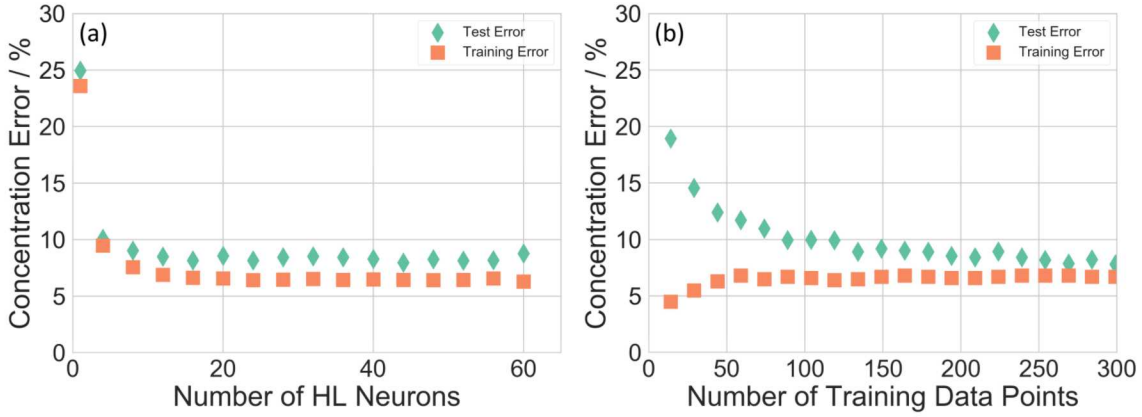

Figure 5. Average test and training error as a function of (a) number of hidden layer neurons and (b) size of the training dataset. Diminishing returns on test error are observed after 16 hidden layer neurons and 150 training data points.

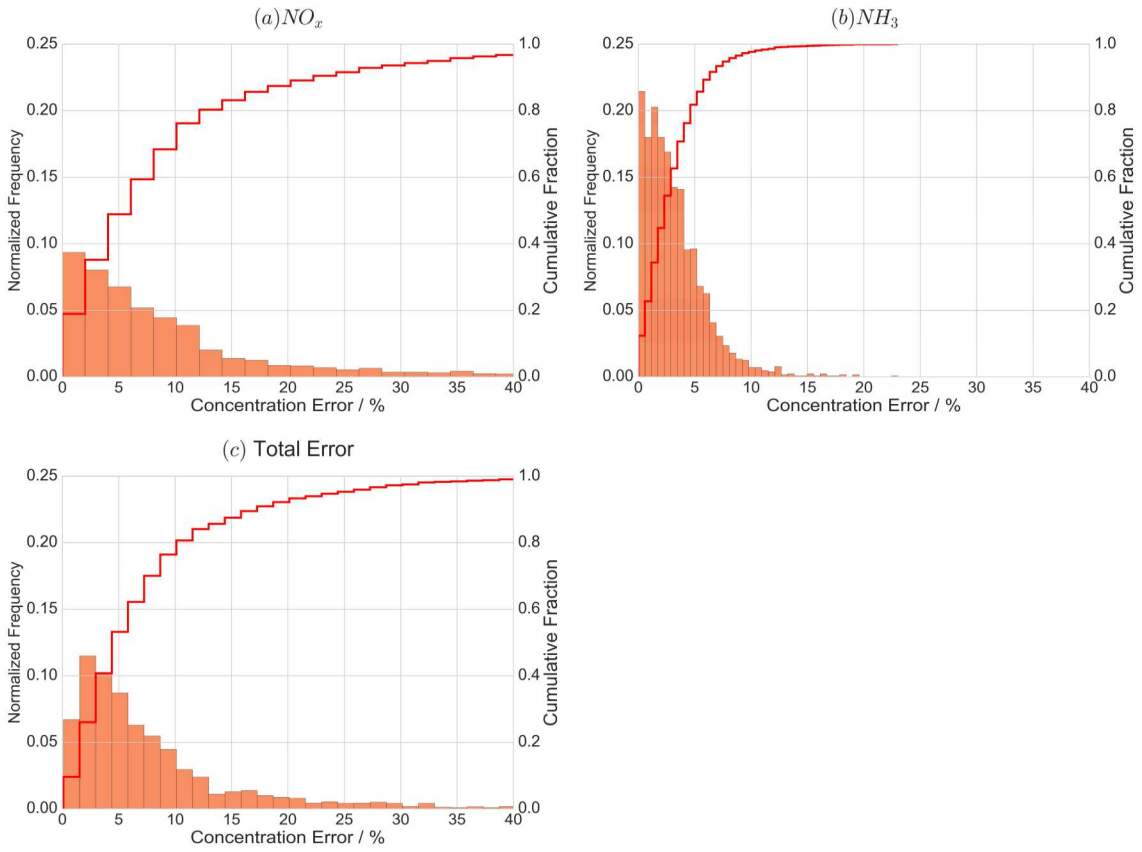

Figure 6. Error histogram for ternary mixtures of NO, NO_2, and NH_3. (a) Shows the error for NO, (b) shows the error for NH_3, and (c) shows the total error. We demonstrate the ability to achieve 90% error bounds of 20% for NO_x, 7% for NH_3, and 15% total.

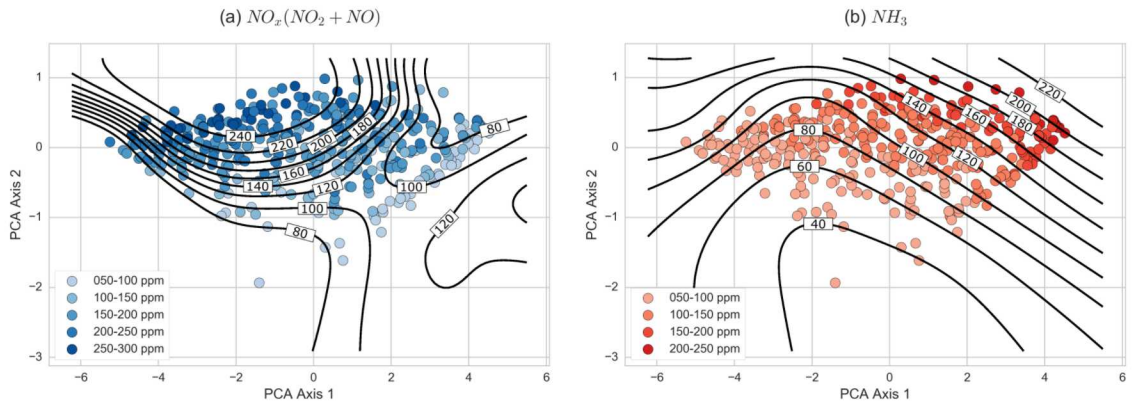

Figure 7. PCA representation of voltage readings compressed from 6D down to 2D for (a) NO_x concentrations and (b) NH_3 concentrations. Contours show predicted concentrations of NO_x and NH_3 generated by an artificial neural network.

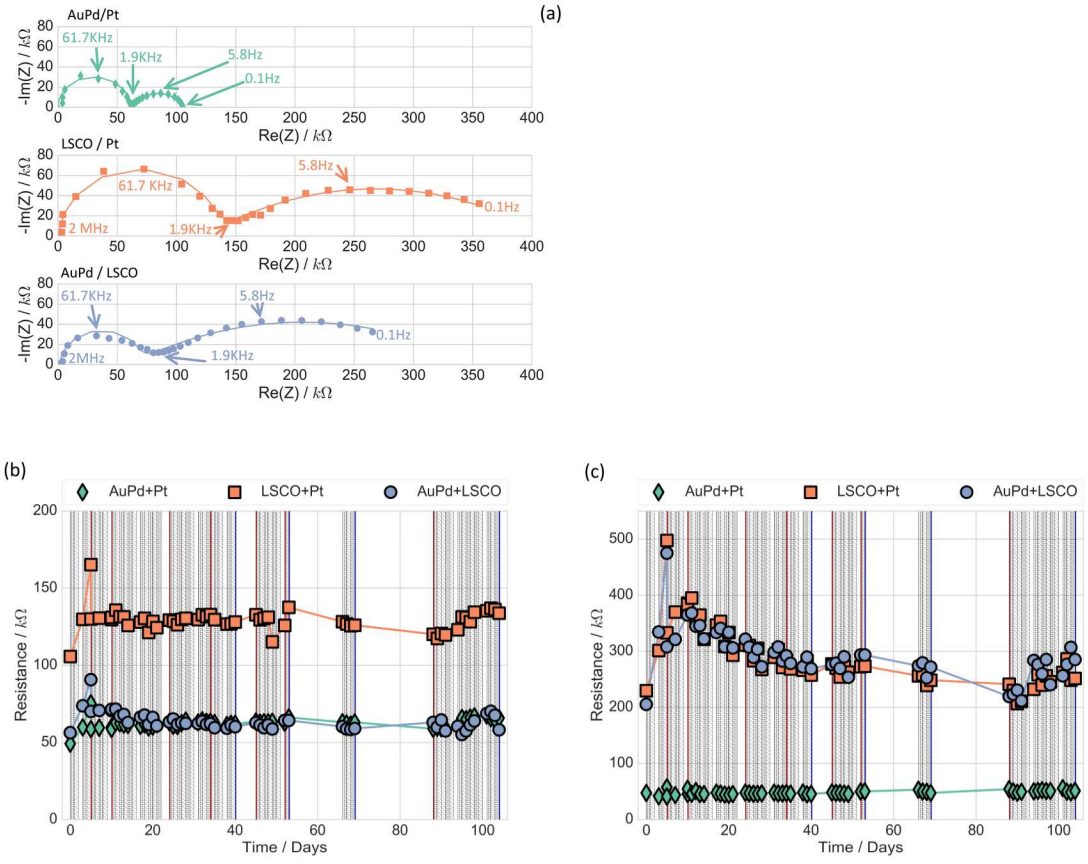

Figure 8. (a) EIS measurements taken on each of the three electrode pairs. (b) Change in R1 and (c) change in R2 resistance as a function of time over the course of the stability test period. Gray areas represent the exposure of the sensors to test gases, and white areas represent periods where the system was shut down.